PCCP

Accepted Manuscript

This is an *Accepted Manuscript*, which has been through the Royal Society of Chemistry peer review process and has been accepted for publication.

Accepted Manuscripts are published online shortly after acceptance, before technical editing, formatting and proof reading. Using this free service, authors can make their results available to the community, in citable form, before we publish the edited article. We will replace this *Accepted Manuscript* with the edited and formatted *Advance Article* as soon as it is available.

You can find more information about *Accepted Manuscripts* in the Information for Authors.

Please note that technical editing may introduce minor changes to the text and/or graphics, which may alter content. The journal's standard Terms & Conditions and the Ethical guidelines still apply. In no event shall the Royal Society of Chemistry be held responsible for any errors or omissions in this *Accepted Manuscript* or any consequences arising from the use of any information it contains.

ROYAL SOCIETY OF CHEMISTRY

www.rsc.org/pccp

SCHOLARONE™
Manuscripts

Physical Chemistry Chemical Physics Accepted Manuscript

Journal Name

ARTICLE

Why $LiFePO_4$ is a Safe Battery Electrode: Coulomb Repulsion Induced Electron-State Reshuffling upon Lithiation

Xiaosong Liu,[a,b†] Yung Jui Wang,[a,c†] Bernardo Barbiellini,[c*] Hasnain Hafiz,[c] Susmita Basak,[c] Jun Liu,[d] Thomas Richardson,[d] Guojiun Shu,[e] Fangcheng Chou,[e] Tsu-Chien Weng,[f] Dennis Nordlund,[f] Dimosthenis Sokaras,[f] Brian Moritz,[g] Thomas Deveraux,[g] Ruimin Qiao,[a] Yi-De Chuang,[a] Arun Bansil,[c] Zahid Hussain[a] and Wanli Yang[a*]

Received 00th January 20xx,
Accepted 00th January 20xx

DOI: 10.1039/x0xx00000x

www.rsc.org/

$LiFePO_4$ is a battery cathode material with high safety standards due to its unique electronic structure. We performed systematic experimental and theoretical studies based on soft x-ray emission, absorption, and hard x-ray Raman spectroscopy of Li_xFePO_4 nanoparticles and single crystals. The results clearly show a non-rigid electron-state reconfiguration of both the occupied and unoccupied Fe-3*d* and O-2*p* states during the (de)lithiation process. We focus on the energy configurations of the occupied states of $LiFePO_4$ and the unoccupied states of $FePO_4$, which are the critical states where electrons are removed and injected during the charge and discharge process, respectively. In $LiFePO_4$, the soft x-ray emission spectroscopy shows that, due to the Coulomb repulsion effect, the occupied Fe-3*d* states with the minority spin sit close to the Fermi Level. In $FePO_4$, the soft x-ray absorption and hard x-ray Raman spectroscopy show that the unoccupied Fe-3*d* states again sit close to the Fermi Level. These critical *3d* electron state configurations are consistent with the calculations based on modified Becke and Johnson potentials GGA+U (MBJGGA+U) framework, which improves the overall lineshape prediction compared with the conventionally used GGA+U method. The combined experimental and theoretical studies show that the non-rigid electron state reshuffling guarantees the stability of Oxygen during the redox reaction throughout the charge and discharge process of $LiFePO_4$ electrodes, leading to the intrinsic safe performance of the electrodes.

Introduction

Olivine-structured $LiFePO_4$, a positive-electrode (cathode) material for rechargeable Li-ion batteries (LIBs), has been commercialized because of its low cost, stable capacity close to the theoretical value (170 mA h g^{-1})[1, 2]. More importantly, when compared with other common transition metal (TM)-based layered compounds, such as $LiCoO_2$, $LiFePO_4$ has long been found to offer high safety, which is critical for the battery applications in large-scale power systems like electric vehicles[3]. The improvement of safety in $LiFePO_4$ is generally attributed to the so-called "inductive effect" of the PO_4 tetrahedron[1]. Fundamentally, the inductive effect reduces the covalent character of the Fe-O bond. Consequently, the Fe 3d and O 2*p* band overlap is avoided [4-6]. It has been known that the overlap of transition-metal and O states presents the main

[a] Advance Light Source, Lawrence Berkeley National Laboratory, Berkeley, CA 94720, USA.
[b] State Key Laboratory of Functional Materials for Informatics, Shanghai Institute of Microsystem and Information Technology, Chinese Academy of Sciences, Shanghai, 200050, P.R.China.
[c] Department of Physics, Northeastern University, Boston, MA 02115, USA.
[d] Environmental Energy Technologies Division, Lawrence Berkeley National Laboratory, Berkeley, CA, 94720, USA.
[e] Center for Condensed Matter Sciences, National Taiwan University, Taipei, 10617 Taiwan.
[f] Stanford Synchrotron Radiation Light Source, SLAC National Accelerator Laboratory, Menlo Park, California 94025, USA.
[g] Stanford Institute for Materials and Energy Sciences, Stanford University and SLAC National Accelerator Laboratory, Menlo Park, California 94025, USA.
† These authors contribute equally to this work.
* Corresponding Authors: B.Amidei@neu.edu (B.B.) and WLYang@lbl.gov (W.Y.)

Electronic Supplementary Information (ESI) available: See
DOI: 10.1039/x0xx00000x

Physical Chemistry Chemical Physics Accepted Manuscript

Please do not adjust margins

concern for the safety in Li_xCoO_2 since it causes oxygen liberation under certain circumstances, e.g. x < 0.5 and/or high temperature[7]. Commercially, the reversible capacity of the $LiCoO_2$ based electrode is only about half of its theoretical value[8] while $LiFePO_4$ can achieve almost the full theoretical capacity[2].

However, even in a simplified scheme with non-overlapping TM-3*d* and anion-*p* states, a detailed configuration of the electronic states is crucial to warrant a safe operation of a battery. A safe battery electrode material requires that the occupied (unoccupied) TM *d* states sit closer to the Fermi Level in the lithiated (delithiated) states, compared with that of the anion *p* states. In this case, the removal (insertion) of electrons through the delithiation (lithiation) process takes place only to the TM[9]. Such scenario has not yet been directly checked in battery electrode materials, and its experimental detection requires techniques that could probe the partial density of state (pDOS) of TM-*d* and anion-*p* for both the occupied and unoccupied bands.

Another important role played by the valence energy levels is to provide an intrinsic limit for the cathode (anode) voltage by pinning of a redox couple at the top of an anion *p*-band (the bottom of cation conduction band)[4, 10, 11]. This scheme is a generalization of the Zaanen-Sawatzky-Allen (ZSA) method[12, 13], which uses the parameters of the Hubbard gap and charge transfer gap for classifying Mott-Hubbard (M-T) and charge-transfer (C-T) insulators. Therefore, the energy configuration of the O-*p* and TM-*d* electron states is a crucial feature associated to the safety and performance of the electrochemical operation. Its relevance for the development of better cathodes in Li-ion battery has been documented in several studies[4, 8, 11, 14].

Li_xFePO_4 is also an ideal candidate to investigate the effect of the strong Coulomb interaction between 3d electrons with opposite spin. Calculations and experiments have revealed that the Fe 3*d* states in Li_xFePO_4 are in the high-spin configuration since the crystal field splitting is smaller than the exchange splitting[15-18]. Upon Li intercalation, the iron 3*d* shell configuration changes from spin saturated $3d^5$ to $3d^6$. In a half-filled high-spin $3d^5$ system, d electrons align their spin because of the first Hund's rule, which is explained by a reduction of Coulomb energy when electrons with same spin are kept apart by the exchange hole as a result of the Pauli's exclusion principle. Therefore, five unpaired electrons per Fe^{3+} ion in $FePO_4$ fill up the t_{2g} and e_g orbitals with the same (majority) spin state. Upon lithiation, electrons enter the TM *3d* states to compensate the positive charge of Li^+ ions, leading to a $3d^6$ system. The injected electron fills the t_{2g} level and adopts the opposite (minority) spin state to satisfy the Pauli's exclusion principle. Such *3d* minority-spin electron injection generate a strong on-site Coulomb energy penalty given by a Coulomb integral involving a pair of electrons with opposite spin occupying the same orbital. This Coulomb energy scale explains the evolution of Fe 3*d* electronic structure upon lithiation and plays a crucial role in electronic structure calculations for several 3*d* TM oxides cathode materials[14, 19]. Incidentally, the same on-site Coulomb integrals are also useful to predict magnetic properties of nano-sized quantum dots[20, 21]. Li_xFePO_4 thus provides an ideal system for a comparative study of the high spin $3d^6$ and $3d^5$ systems involving on-site Coulomb integrals.

To extract the aforementioned electronic states in the vicinity of the Fermi level, including both the occupied and unoccupied pDOS of Fe-*3d* and O-*2p* states in Li_xFePO_4, we performed soft x-ray emission spectroscopy (sXES), soft x-ray absorption spectroscopy (sXAS), and Hard x-ray Raman spectroscopy (hXRS) on Li_xFePO_4 nanoparticles and $LiFePO_4$ single crystals. The results reveal the reshuffling of the Fe-3*d* valence states upon lithiation due to the strong Coulomb interaction between 3d electrons with opposite spin. In order to generate the theoretical pDOS of Fe-*3d* and O-*2p* states, we used density functional theory (DFT) calculations with the generalized gradient approximation (GGA) + *U* and the modified Becke and Johnson potentials GGA (MBJ-GGA)[22]. The GGA provides a simple yet accurate step beyond the local density approximation (LDA) to describe magnetic ground-state properties of metallic iron[23] while corrections due to strong Coulomb interactions between localized TM-3*d* electrons in Li_xFePO_4 can be captured with a Hubbard term *U*[24-26]. Besides, the MBJ potential offers an efficient way to correct semilocally quasi-particle energies in insulators and semiconductors. While the DFT + *U* has been the most widely used correlation scheme in the Li-ion battery field [19, 27-29], the MBJ-GGA yields band gaps[22] with an accuracy comparable to sophisticated quasi-particle methods based on many body perturbation theory. DFT + *U* has accurately predicted various key properties of $LiFePO_4$, such as the band gap[30], the Li intercalation voltage[30], the phase separation[30], the elastic properties[31] and the transport of small polarons[32]. However, limitations of the DFT + *U* approach are still under scrutiny[33]. In this work we show that the MBJ-GGA+U by enabling relevant quasi-particle corrections displays the best overall agreement with sXES, sXAS and hXRS spectroscopic data, which allows us to extract the electronic structure that characterizes the safety and performance of the Li_xFePO_4 electrodes.

Experimental and theoretical Procedures

The Li_xFePO_4 (0 < x < 1) nanoparticles and $LiFePO_4$ single crystals are from the same batch used in our previous work, in which the sample preparation, storage, and transportation were described in details[18]. The soft X-ray (sXES, sXAS) and hard X-ray (hXRS) experiments are performed at the Advanced Light Source (ALS) of Lawrence Berkeley National Laboratory (LBNL) and the Stanford Synchrotron Radiation Lightsource (SSRL), respectively. sXES involves a core-electron excitation and the decay of this excited state by emission of an X-ray photon. The spectra provide the information of occupied valence electrons that fill the core hole during the decay process[34]. The sXAS complements sXES since it measures the absorption of the incident photon by a specific core electron excited into an unoccupied state. For $LiFePO_4$, sXES and sXAS directly detect the occupied and unoccupied O-*2p* and Fe-*3d* states, respectively, through dipole allowed transitions[34].

Physical Chemistry Chemical Physics Accepted Manuscript

This journal is © The Royal Society of Chemistry 20xx

Please do not adjust margins

While the probe depth of sXES is about 100 nm, it is only about 10 nm for sXAS collected through the total electron yield (TEY)[9]. We thus perform hXRS for the complementary bulk information on the unoccupied states with probe depth of several micrometers. hXRS at low moment transfer geometry is analogous to the sXAS[35], but without the self-absorption issue incurred by the total fluorescence yield (TFY) of sXAS[36]. We should mention that other techniques such as the X-ray photoemission spectroscopy (XPS) are able to map the occupied total DOS and has delivered important information[37], however, compared with the combination of sXES and sXAS, they do not resolve the partial contributions of each elements experimentally, and do not probe the unoccupied states. Therefore, the combination of sXES, sXAS and hXRS can be considered the tool-of-choice for studying both the occupied and unoccupied electronic states of battery materials with elemental and orbital sensitivity[9].

Our DFT calculations were performed within the linear augmented-plane-wave (LAPW) method provided by the WIEN2K package[38]. The GGA of Perdew et al[39] and MBJ potentials[22] were used to describe the exchange-correlation potential. Orthorhombic $LiFePO_4$ and $FePO_4$, containing 28 and 24 atoms respectively, were initialized in antiferromagnetic configurations. All calculations were performed at the experimental lattice parameters[40]. The largest plane-wave vector K_{max} was determined by setting $R_{MT}K_{max} = 7$, and the integrals over the Brillouin zone were performed using a tetrahedron method on a mesh of 4×4×2 k-points. The charge convergence of 0.0001e was used for the self-consistency. The Hubbard term *U* was introduced for calculating Fe-3d since the standard DFT in either LDA or GGA implementations is insufficient to capture strong Coulomb interactions for localized *d*-electrons of the TM elements in highly correlated systems[41]. The DFT + *U* method can be then used as a cure by adding to the DFT Hamiltonian a term with a site dependent Hubbard parameter *U*. While the values of U is found to be about 4 eV in the previous GGA+U studies[37, 41, 42], values of *U* of 1 eV and 3 eV are used for MBJGGA+U calculations of $LiFePO_4$ and $FePO_4$, respectively, in order to be consistent with the band gap values[37, 43]. While the Fe-*L* sXES allows the visualization of the non-rigid electron state reshuffling, the spectroscopic process involves excitations of electrons and does not correspond directly to the electronic ground state. In order to extract the ground state configuration of $LiFePO_4$ and $FePO_4$, we simulate our experimental sXES results with DFT calculations of both the Fe-*3d* and O-*2p* pDOS. The theoretical sXES simulation were performed within a method [44] implemented in WIEN2K.

Results and Discussion

Fig.1 shows the Fe L_3-edge sXES spectra of a serial of Li_xFePO_4 with different Li contents. These spectra correspond to the occupied Fe-*3d* electrons decaying to the $2p^{3/2}$ core holes[34]. The overall spectral lineshape of the two end members, $LiFePO_4$ and $FePO_4$, is in agreement with previous studies[17, 45]. Compared with $FePO_4$, sXES from $LiFePO_4$ displays a shift of 1.3 eV on the main emission peak towards lower energy, in addition to an extra feature at around 709 eV. The intensity of this hump displays a monotonic damping upon delithiation. Two isosbestic points could be clearly identified if we stack all the sXES spectra together (two arrows in Fig.1(b)) They reveal a two-phase transformation, which has been discussed in details previously based on Fe-*L* absorption data[18]. Here, we are able to fit well the sXES data of the intermediate doping concentrations x=0.3 and 0.7, through a simple linear combination of the spectra of $LiFePO_4$ and $FePO_4$. The fitted spectra are illustrated in Figure 1(a) (open circles) and they fully overlap the experimental data. This excellent fitting confirms again the two-phase scenario in our chemically prepared Li_xFePO_4 samples. The fitting yields quantitative Li concentration values of x = 0.70 and 0.32, higher than the values, 0.48 and 0.19, found through the sXAS analysis[18]. This discrepancy is due to the different probing depths of XAS (10 nm) and sXES (100 nm). Thus the comparison between sXES and sXAS results indicates a higher concentration of Li in the bulk than that on the surface, which is consistent with the previous studies[46].

The two isosbestic points in Fig.1(b), at about 706.8 and 709 eV, indicate the presence of three monotonic trends in the spectroscopy[47], corresponding to three occupied electron states. These three states can be better visualized through multi-peak fittings, as shown in Fig. 2(a). The spectrum of $FePO_4$ is well fitted by a single Gaussian function (centroid = 707.1 eV, FWHM = 2.7 eV). The high-energy hump and the asymmetric lineshape of the $LiFePO_4$ spectrum requires the use of several Gaussian functions to obtain a good agreement. A good fit is achieved when using three components as 1) centroid = 706 eV, FWHM = 2.1 eV, 2) centroid = 707.5 eV, FWHM = 2.7 eV, and 3) centroid = 709 eV, FWHM = 2.3 eV, with the ratio of the maxima 0.86: 0.1: 0.3. This analysis is rationalized by the following physics arguments. First, the FWHM of all Gaussian functions must be comparable because the broadening effect from the core-hole lifetime and instrumentation remains the same. Second, the 707.5 eV low-intensity feature of $LiFePO_4$ is close to $FePO_4$, which indicates a small contribution from the $FePO_4$ on the surface[18, 46]. The small energy shift of this feature, compared with the main feature of $FePO_4$ (707.1 eV), is likely due to the chemical potential shift. Third, the features at 706 and 709 eV correspond to a "divided" configuration of the Fe-*3d* ($3d^6$) states in $LiFePO_4$, contrasting the "integrated" configuration of the $3d^5$ states at 707.3 eV in $FePO_4$.

It is known that Fe-3*d* states in Li_xFePO_4 are in the high-spin configuration[15-18]. The five Fe-3*d* electrons in $FePO_4$ half-fill the five *3d* orbitals with the same majority spin state. The extra electron introduced in $LiFePO_4$ has to take the opposite minority spin, which triggers a strong on-site Coulomb interaction, resulting in the splitting of the electron state configuration in $LiFePO_4$. Therefore, by probing the pDOS of the Fe-*3d* occupied states, our Fe-L_3 sXES spectrum experimentally visualize a lithiation-induced Coulomb

Physical Chemistry Chemical Physics Accepted Manuscript

interaction, which leads to the redistribution of the electron states. The energy of the on-site Coulomb repulsion is determine by the gap dividing the Fe-*3d* features of $LiFePO_4$, i.e., $U_{on\text{-}site}$ = 3.0 eV.

Fig.2 and Fig.3 show the simulated Fe-*L* and O-*K* sXES spectra of $LiFePO_4$ and $FePO_4$ by including dipole matrix elements for the transition between core and valence states, in comparison with the experimental data. The Fe-2p and O-1s core energies can be estimated from atomic calculations, but for the sake of simplicity, our calculated results are lined up to the experimental spectra. We compare the calculations with the GGA+U method with *U* varying from 0 eV to 8 eV by steps of 1 eV. The results for the Fe-*L* sXES profiles with nine different values of U are presented in Fig.2 (c-d). Calculations of sXES using the MBJGGA+U method for $LiFePO_4$ (with *U*=1 eV) and $FePO_4$(*U*=3eV) are plotted with the experimental data at the bottom of each panel.

For $LiFePO_4$ (Fig.2c), the GGA+U calculation with U = 0 eV shows a mean peak at 706 eV and a clear shoulder at about 2 eV above the mean peak, in qualitatively agreement with the experiment. However, as the value of U increases, the mean peak becomes broader and the spectral weight shifts toward lower energy. For $FePO_4$ (Fig.2d), the GGA+U calculation with U = 0 eV shows a significant spectral weight above 710 eV, which does not agree with the experimental data. This discrepancy decreases as the value of U increases.

The pDOS information detected by sXES enables a direct comparison between the theory and experiments. The GGA (U=0) bandgap of $LiFePO_4$ and $FePO_4$ are 0.5 eV and 0.8 eV respectively and the mean 3d valence states peak of $FePO_4$ corresponding to U = 0 eV is 3 eV below Fermi energy (Fig. S1). The 0.5 eV bandgap of $LiFePO_4$ is too small compared with the experimental gap obtained in optical measurements[48]. Using a finite U improves the band gap evaluation, as also observed in a previous report[30]. However, GGA+U calculations with these optimal U values are generally not consistent with our spectroscopic data in terms of the overall lineshapes (Fig. S2), as also reported previously[37]. In contrast, the MBJGGA+U method optimizes both the bandgap and the overall lineshape.

Therefore, our comparison between the calculations and sXES experiments indicate that the Hubbard U correction alone is not sufficient to explain both the band gap and the overall band structure. Further quasi-particles has to be included, through MBJGGA+U, to allow more flexibility to reproduce the shape of the spectroscopic results.

Fig. 3(a) shows the O-*K* *s*XES spectra of all samples. In this case, the most significant and systematic change is given by the intensity of the low energy shoulder at 524.5 eV, which shows a monotonic decrease upon delithiation. The gradual change on the 524.5 eV shoulder intensity upon lithiation is in agreement with the two-phase analysis for the Fe-*L* data discussed above. As shown in Fig. 3(b-c), the calculated O-*K* sXES lineshape in both $FePO_4$ and $LiFePO_4$ is less sensitive to the variation of U. Nevertheless, the MBJGGA+U results, using the same parameters as for the Fe-*L* sXES simulations, are again in fair agreement with the experimental data. This agreement between our MBJGGA+U and the experiment validates the pDOS MBJGGA+U calculations. Besides, MBJGGA+U calculations predict that $LiFePO_4$ and $FePO_4$ have a band gap of about 3.6 eV in agreement with previous studies[37, 43].

Fig.4 shows the spin-polarized Fe-3*d* (4 atoms) and O-2*p* pDOS (16 atoms) of $LiFePO_4$ and $FePO_4$. The Fermi energy is set at 0 eV. As shown in Fig.4(b), the calculated Fe-3*d* pDOS shows that the d electrons of $FePO_4$ are all in spin-up states. This is expected for Fe^{3+} high-spin $3d^5$ configuration[15-18]. In $LiFePO_4$ (Fig. 4(a)), an extra valence electron is needed to neutralize the intercalated Li ion. This extra electron fills one of t_{2g} orbital and must be in a spin-down state, which results in a strong on-site Coulomb interaction. This Coulomb energy penalty lowers the band of the majority spin-up states and reshuffles the entire valence electronic structure. Such a non-rigid band scenario is critical for battery materials since the extra electron in the Fe-*3d* minority spin-down state sits very close to the Fermi level, as clearly predicted by the calculations (Fig. 4(a)) and experimentally observed as a hump located at high energy (709 eV) in the Fe-*L* sXES of $LiFePO_4$ (Fig.1, Fig.2). Therefore under such a senario, removing electrons from $LiFePO_4$ during the delithiation process will take place in the occupied Fe-3d states, and thus, a direct involvement of O-2p states is avoided.

The delithiation (charging) process of $LiFePO_4$ is fundamentally regulated by the electronic configuration of its *occupied* states, where electrons will be removed. On the other hand, the lithiation (discharging) process is defined by the *unoccupied* states, where the electrons will be injected. The unoccupied electronic states are measured by sXAS and hXRS[34]. Previously, we have studied in detail the Fe-*L* sXAS of Li_xFePO_4. The Fe-*L* spectrum is dominated by atomic multiplet effects with abundant information on the valence, crystal fields, and phase transformation[18]. Our focus in this work is to determine the relative energy positions of the unoccupied Fe-*3d* and O-*K* states, which is essential for understanding the lithiation (discharging) process during battery operations.

It has been established that, in *3d* TM compounds, the relatively sharp low-energy O-*K* sXAS features, the so-called "pre-edge features" or "in-gap states"[49], are of mainly TM-*3d* character. They arise from the covalent mixing (hybridization) of the TM-*d* and anion-*p* states[34, 49, 50]. Therefore, a well-defined pre-edge peak in O-*K* sXAS indicates that the TM-*3d* states sit close to the Fermi level and inside the band gap of the broad O-*2p* bands. Fig. 5(a) presents the sXAS of O-*K* edge collected on the $LiFePO_4$ single crystals, nanoparticles, and $FePO_4$ nanoparticles. The "pre-edge" hybridization feature at 530-533 eV is obvious for $FePO_4$, but very weak for $LiFePO_4$ in both the nanoparticles and single crystals. This is consistent with the previous experiments[17], but it has been unclear whether the weak pre-edge feature of $LiFePO_4$ is intrinsic or from the surface effect.

As the sXAS in TEY mode detects only the top 10 nm surface, we perform hXRS experiment to clarify the origin of the weak pre-edge feature of $LiFePO_4$[18, 46]. The hXRS results with several

Physical Chemistry Chemical Physics Accepted Manuscript

This journal is © The Royal Society of Chemistry 20xx

Please do not adjust margins

micrometer probe depth, as in Fig. 5(b), shows that the (bulk) single crystal $LiFePO_4$ does not show any pre-edge feature after integrating the data for more than 2 hours. hXRS of the nanoparticles displays a low intensity of the pre-edge due to the large surface to bulk ratio for nanoparticles. Therefore, our hXRS result of the $LiFePO_4$ single crystals clarifies that the weak O-*K* sXAS pre-edge feature observed in $LiFePO_4$ is not an intrinsic feature, but stems from a surface effect, likely the Li deficiency. It is important to note that the non-existing pre-edge feature does not contradict the theoretical calculations, where the Fe-*3d* states sit below the O-*2p* bands for both $LiFePO_4$ and $FePO_4$ (Fig.4). Introducing Li-ions into the $FePO_4$ drives the system into a highly ionic state, which greatly suppresses the Fe-O covalent features. Therefore, it is the reduction of Fe-O hybridization that results in the disappearance of the O-*K* pre-edge feature in $LiFePO_4$. For $FePO_4$, the pre-edge feature around 530-533 eV remain strong for both the sXAS and hXRS tests (Fig.5 a,b). Such a consistency between the $FePO_4$ sXAS and hXRS on the Fe-O hybridization feature show that, for the unoccupied electron states in $FePO_4$, the Fe-*3d* states intrinsically sit close to Fermi level and below the broad O-K bands.

Fig.6 summarizes our sXES (Fig.1, 2), sXAS and hXRS (Fig.5) studies into a schematic diagram of the electron states that are involved in the charge/discharge process of Li_xFePO_4. The occupied states in $LiFePO_4$ are critical for the charging (delithiation) process, where electrons will be removed. Due to the Coulomb interactions, the Fe-3d electrons with minority spins in $LiFePO_4$ are "pushed" up in energy and sit close to Fermi level. So the electrons will be removed from these Fe-3d states during the electrochemical charge. This high-energy Fe-3d state is evidently shown by the sXES experimental data (red arrow in Fig.6). For the discharging (lithiation) process, the unoccupied states in $FePO_4$ becomes more important. Again, hard x-ray XRS data show that the intrinsic unoccupied Fe-*3d* state sits close to the Fermi level. Therefore, both the charging and discharging process involve almost purely the Fe-3d states in the $LiFePO_4$ system. Because the active electrons are highly localized to the Fe-*3d* orbitals, there is minimum involvement of the Oxygen state, leading to the safe electrochemical operations. Additionally, the formal valence of Fe is much better defined in $LiFe^{(II)}PO_4$ and $Fe^{(III)}PO_4$ with a clear two-phase distribution, contrasting many other transition metals used in battery cathodes that display a fluctuation in valences and/or mixture (solid-solution type) of charges involving a finite contribution from the anion[51]. We would like to emphasize that such a special electronic state configuration is *not* simply due to the number of *3d* electrons, i.e., the valences; instead, it is a result of the interplay of the local crystal field surrounding the TM and the spin states of the electrons, as also shown recently in the Mn- and Fe- based Prussian Blue analogues[52, 53]. By virtue of the sensitivity to the electron states with elemental, orbital, and site sensitivities, sXES and sXAS, with theoretical calculations, are demonstrated in this work as the tools-of-choice for revealing the detailed electronic configuration of both the occupied and unoccupied states in the vicinity of the Fermi level.

Conclusions

Through the combined spectroscopic and theoretical studies, we provide a comprehensive understanding of the safe operation of $LiFePO_4$ materials as a battery electrode, from the electronic structure point of view. For the lithiated state in $LiFePO_4$, the Fe-*L* sXES and theory shows an occupied minority-spin Fe-3*d* state that is separated from the majority-spin state and sits at high energy close to the Fermi level. This is due to an electronic reshuffling induced by strong Coulomb interactions of Fe-*3d* electrons with opposite spins. When $LiFePO_4$ is charged (delithiated), only these minority spin Fe-*3d* electrons are removed since they are close to the Fermi level. For the delithiated state in $FePO_4$, the O-*K* sXAS and hXRS demonstrate that the unoccupied Fe-*3d* states sit in the band gap of the O-2*p* bands, again close to the Fermi level. When $FePO_4$ is discharged (lithiated), electrons are introduced into these empty minority-spin Fe-*3d* states, and reshuffle the electronic configuration as described for $LiFePO_4$. In both cases, the charge transfer involves only Fe-*3d* states. This mechanism intrinsically stabilizes the oxygen states throughout the electrochemical operation.

Our work clearly demonstrates that the electronic structure associated with the electrode charge/discharge process can be revealed through a combined spectroscopic and theoretical analysis. The electronic states in the vicinity of the Fermi level play a crucial role in the design and operation of Li-insertion cathodes. In fact, such consideration has led to the inventions of both the $LiFePO_4$ and $LiCoO_2$ cathodes, as directly testified by Goodenough[54]. Since most of the Lithium ion battery cathodes are *3d* TM compounds, our results not only clarify the mechanism leading to the safe operation of the $LiFePO_4$ cathode from the electronic structure point of view, but also provide a general scheme with demonstrated techniques for understanding and optimizing *3d* TM based battery electrode materials.

Acknowledgements

The Advanced Light Source is supported by the Director, Office of Science, Office of Basic Energy Sciences, of the U.S. Department of Energy under Contract No. DE-AC02-05CH11231. The work at Northeastern University is supported by the U.S. Department of Energy under contract no. DEFG02-07ER46352 and benefitted from allocation of computing time at the NERSC and NU-ASCC computation centers. Use of the Stanford Synchrotron Radiation Lightsource, SLAC National Accelerator Laboratory, is supported by the U.S. Department of Energy, Office of Science, Office of Basic Energy Sciences under Contract No. DE-AC02-76SF00515. X.L. is supported by the National Natural Science Foundation of China (21473235, 11227902), One Hundred Person Project of the Chinese

Physical Chemistry Chemical Physics Accepted Manuscript

Academy of Sciences, and Shanghai Pujiang Program (14PJ1410400). R.Q. is supported by the Lawrence Berkeley National Laboratory LDRD program.

Author Contributions

X.L., R.Q., Y.C., Z.H. and W.Y. performed the spectroscopic measurements. T.W. D.N. and D.S. performed the hard X-ray Raman measurements. J.L. and T.R. prepared the nanoparticles. G.S. and F.C. prepared the single crystals. B.B., T.D. and A.B. supervised the first-principles calculations, which were performed by Y.W., H.H., S.B. and B.M.. All authors contributed to the data analysis and scientific discussions. X.L., Y.W., B.B., and W.Y. wrote the manuscript with contributions from all the authors.

Notes and references

1. A. K. Padhi, K. S. Nanjundaswamy and J. B. Goodenough, *Journal of The Electrochemical Society*, 1997, 144, 1188-1194.
2. G. R. Dahlin and K. E. Strøm, *Lithium batteries : research, technology, and applications*, Nova Science Publishers, New York, 2010.
3. D. D. MacNeil, Z. Lu, Z. Chen and J. R. Dahn, *Journal of Power Sources*, 2002, 108, 8-14.
4. G.-A. Nazri and G. Pistoia, *Lithium Batteries: Science and Technology*, Springer Verlag, 2009.
5. L.-X. Yuan, Z.-H. Wang, W.-X. Zhang, X.-L. Hu, J.-T. Chen, Y.-H. Huang and J. B. Goodenough, *Energy & Environmental Science*, 2011, 4, 269-284.
6. A. K. Padhi, K. S. Nanjundaswamy, C. Masquelier, S. Okada and J. B. Goodenough, *Journal of The Electrochemical Society*, 1997, 144, 1609-1613.
7. J. R. Dahn, E. W. Fuller, M. Obrovac and U. Von Sacken, *Solid State Ionics*, 1994, 69, 265-270.
8. B. L. Ellis, K. T. Lee and L. F. Nazar, *Chemistry Of Materials*, 2010, 22, 691-714.
9. W. Yang, X. Liu, R. Qiao, P. Olalde-Velasco, J. D. Spear, L. Roseguo, J. X. Pepper, Y.-d. Chuang, J. D. Denlinger and Z. Hussain, *Journal of Electron Spectroscopy and Related Phenomena*, 2013, 190, 64-74.
10. J. B. Goodenough and Y. Kim, *Journal of Solid State Chemistry*, 2009, 182, 2904-2911.
11. J. B. Goodenough and Y. Kim, *Chemistry Of Materials*, 2010, 22, 587-603.
12. J. Zaanen, G. A. Sawatzky and J. W. Allen, *Physical Review Letters*, 1985, 55, 418-421.
13. P. Olalde-Velasco, J. Jiménez-Mier, J. Denlinger, Z. Hussain and W. Yang, *Physical Review B*, 2011, 83, 241102.
14. J. Reed and G. Ceder, *Chemical Reviews*, 2004, 104, 4513-4533.
15. A. Yamada and S. C. Chung, *Journal of The Electrochemical Society*, 2001, 148, A960-A967.
16. S. Shi, C. Ouyang, Z. Xiong, L. Liu, Z. Wang, H. Li, D.-s. Wang, L. Chen and X. Huang, *Physical Review B*, 2005, 71, 144404.
17. A. Augustsson, G. V. Zhuang, S. M. Butorin, J. M. Osorio-Guillen, C. L. Dong, R. Ahuja, C. L. Chang, P. N. Ross, J. Nordgren and J. H. Guo, *The Journal of chemical physics*, 2005, 123, 184717.
18. X. Liu, J. Liu, R. Qiao, Y. Yu, H. Li, L. Suo, Y. S. Hu, Y. D. Chuang, G. Shu, F. Chou, T. C. Weng, D. Nordlund, D. Sokaras, Y. J. Wang, H. Lin, B. Barbiellini, A. Bansil, X. Song, Z. Liu, S. Yan, G. Liu, S. Qiao, T. J. Richardson, D. Prendergast, Z. Hussain, F. M. de Groot and W. Yang, *Journal of the American Chemical Society*, 2012, 134, 13708-13715.
19. Y. S. Meng and M. E. Arroyo-de Dompablo, *Energy & Environmental Science*, 2009, 2, 589.
20. A. Bansil, D. Nissenbaum, B. Barbiellini and R. Saniz, *Journal of Physics and Chemistry of Solids*, 2004, 65, 2005-2009.
21. R. Saniz, B. Barbiellini, A. Denison and A. Bansil, *Physical Review B*, 2003, 68, 165326.
22. F. Tran and P. Blaha, *Physical Review Letters*, 2009, 102, 226401.
23. B. Barbiellini, E. G. Moroni and T. Jarlborg, *Effects of gradient corrections on electronic structure in metals*, Institute of Physics Publishing, 1990.
24. V. I. Anisimov, J. Zaanen and O. K. Andersen, *Physical Review B*, 1991, 44, 943-954.
25. A. I. Liechtenstein and J. Zaanen, *Physical Review B*, 1995, 52, R5467-R5470.
26. V. I. Anisimov, F. Aryasetiawan and A. I. Lichtenstein, *Journal Of Physics-Condensed Matter*, 1997, 9, 767-808.
27. G. Ceder, *Mrs Bulletin*, 2010, 35, 693-701.
28. G. Ceder, G. Hautier, A. Jain and S. P. Ong, *Mrs Bulletin*, 2011, 36, 185-191.
29. G. Hautier, A. Jain, S. P. Ong, B. Kang, C. Moore, R. Doe and G. Ceder, *Chemistry Of Materials*, 2011, 23, 3495-3508.
30. F. Zhou, M. Cococcioni, K. Kang and G. Ceder, *Electrochemistry Communications*, 2004, 6, 1144-1148.
31. T. Maxisch and G. Ceder, *Physical Review B*, 2006, 73, 174112.
32. T. Maxisch, F. Zhou and G. Ceder, *Physical Review B*, 2006, 73, 104301.
33. R. C. Albers, N. E. Christensen and A. Svane, *Journal of physics. Condensed matter : an Institute of Physics journal*, 2009, 21, 343201.
34. F. de Groot and A. Kotani, *Core Level Spectroscopy of Solids*, CRC Press Taylor & Francis Group, Boca Raton, 2008.
35. D. Sokaras, D. Nordlund, T.-C. Weng, R. A. Mori, P. Velikov, D. Wenger, A. Garachtchenko, M. George, V. Borzenets, B. Johnson, Q. Qian, T. Rabedeau and U. Bergmann, *Review of Scientific Instruments*, 2012, 83, 043112.
36. A. J. Achkar, T. Z. Regier, H. Wadati, Y. J. Kim, H. Zhang and D. G. Hawthorn, *Physical Review B*, 2011, 83, 081106.
37. L. Castro, R. Dedryvere, M. El Khalifi, P. Lippens, J. Breger, C. Tessier and D. Gonbeau, *Journal Of Physical Chemistry C*, 2010, 114, 17995-18000.
38. P. Blaha, K. Schwarz, G. K. H. Madsen, D. Kvasnicka and J. Luitz, *WIEN2k, An Augmented Plane Wave + Local Orbitals Program for Calculating Crystal Properties*, Universit at Wien, Austria, Universit at Wien, Austria, 2001.
39. J. P. Perdew, K. Burke and M. Ernzerhof, *Physical Review Letters*, 1996, 77, 3865-3868.
40. G. Rousse, J. Rodriguez-Carvajal, S. Patoux and C. Masquelier, *Chemistry Of Materials*, 2003, 15, 4082-4090.
41. F. Zhou, K. S. Kang, T. Maxisch, G. Ceder and D. Morgan, *Solid State Communications*, 2004, 132, 181-186.

Physical Chemistry Chemical Physics Accepted Manuscript

This journal is © The Royal Society of Chemistry 20xx

Please do not adjust margins

42. F. Zhou, M. Cococcioni, C. Marianetti, D. Morgan and G. Ceder, *Physical Review B*, 2004, 70, 235121.
43. M. K. Kinyanjui, P. Axmann, M. Wohlfahrt-Mehrens, P. Moreau, F. Boucher and U. Kaiser, *Journal of physics. Condensed matter : an Institute of Physics journal*, 2010, 22, 275501.
44. K. Schwarz and E. Wimmer, *Journal of Physics F: Metal Physics*, 1980, 10, 1001-1012.
45. A. Hunt, W. Y. Ching, Y. M. Chiang and A. Moewes, *Physical Review B*, 2006, 73, 205120.
46. J. F. d. r. Martin, A. Yamada, G. Kobayashi, S.-i. Nishimura, R. Kanno, D. Guyomard and N. Dupré, *Electrochemical and Solid-State Letters*, 2008, 11, A12.
47. J. G. Powles and M. L. Williams, *Chemical Physics Letters*, 1989, 156, 543-544.
48. R. Shahid and S. Murugavel, *Phys Chem Chem Phys*, 2013, 15, 18809-18814.
49. F. M. F. de Groot, M. Grioni, J. C. Fuggle, J. Ghijsen, G. A. Sawatzky and H. Petersen, *Physical Review B*, 1989, 40, 5715-5723.
50. P. Olalde-Velasco, J. Jimeacutenez-Mier, J. Denlinger and W.-L. Yang, *Physical Review B*, 2013, 87, 245136.
51. K. Suzuki, B. Barbiellini, Y. Orikasa, N. Go, H. Sakurai, S. Kaprzyk, M. Itou, K. Yamamoto, Y. Uchimoto, Y. J. Wang, H. Hafiz, A. Bansil and Y. Sakurai, *Physical Review Letters*, 2015, 114, 087401.
52. D. Asakura, Y. Nanba, M. Okubo, Y. Mizuno, H. Niwa, M. Oshima, H. Zhou, K. Okada and Y. Harada, *The Journal of Physical Chemistry Letters*, 2014, 5, 4008-4013.
53. L. Wang, J. Song, R. Qiao, L. A. Wray, M. A. Hossain, Y. D. Chuang, W. Yang, Y. Lu, D. Evans, J. J. Lee, S. Vail, X. Zhao, M. Nishijima, S. Kakimoto and J. B. Goodenough, *Journal of the American Chemical Society*, 2015, 137, 2548-2554.
54. J. B. Goodenough, *Chapter 4 Advances in Lithium Ion batteries*, Springer, 2002.

Physical Chemistry Chemical Physics Accepted Manuscript

Please do not adjust margins

Journal Name

ARTICLE

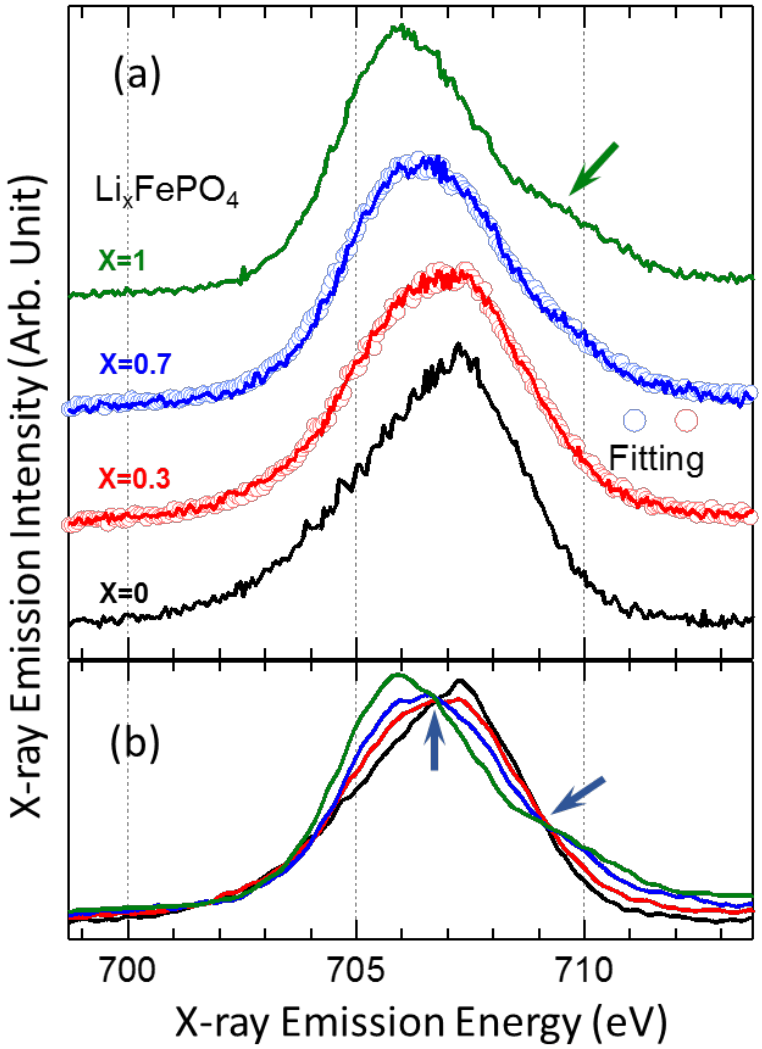

Fig.1 Soft X-ray emission spectroscopy of the Fe-L_3 edges of a series of Li_xFePO_4 nanoparticles. (a) The fittings (open circles) of the intermediate states are performed by linear combinations of the spectra of x=0 ($FePO_4$) and 1 ($LiFePO_4$). The best fittings of the spectra are obtained when the concentration of $LiFePO_4$ is 0.3 and 0.7, which are presented as the x values. Green arrow indicates the extra emission feature in $LiFePO_4$. (b) Two isosbestic points (blue arrows) are obvious when all the sXES data are stacked together.

Physical Chemistry Chemical Physics Accepted Manuscript

This journal is © The Royal Society of Chemistry 20xx

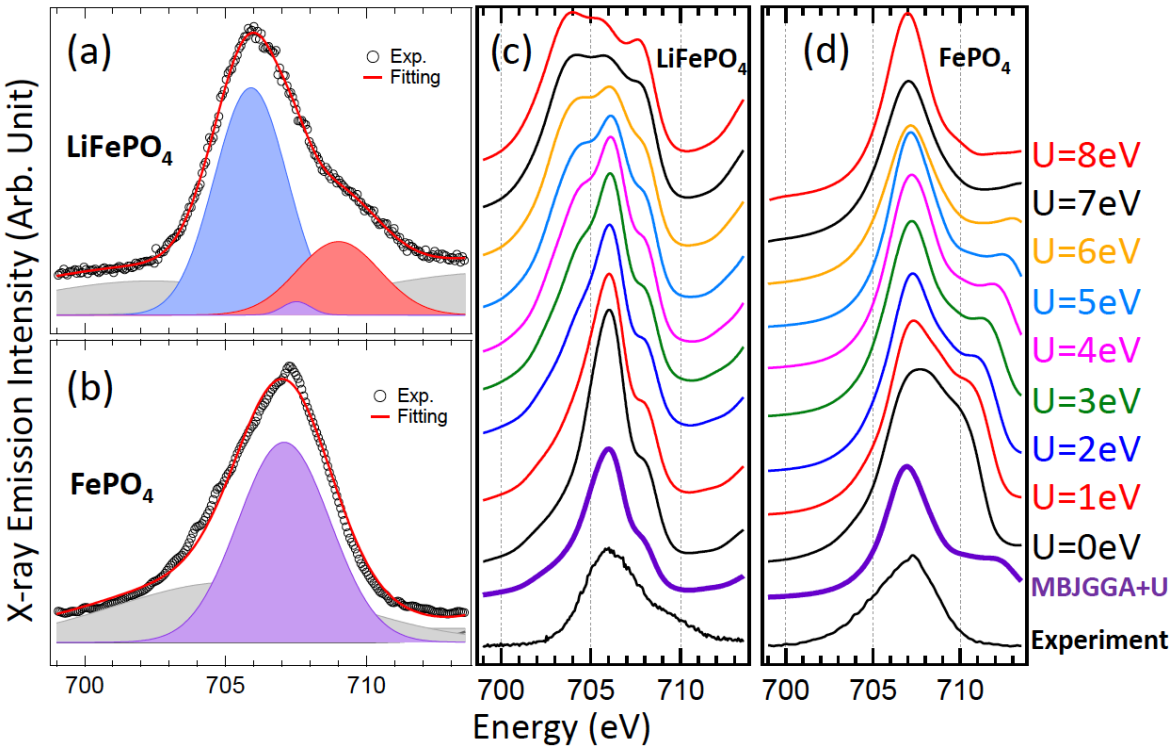

Fig.2. Peak fittings of the experimental Fe-L_3 sXES data of (a) $LiFePO_4$ and (b) $FePO_4$. The sXES features of $LiFePO_4$ include a low-intensity $FePO_4$ feature at 707 eV, and two spited features at 706 and 709 eV. (c) and (d) are theoretical calculations of Fe-L_3 sXES of $LiFePO_4$ and $FePO_4$, respectively. Spectra with the U values of 0 to 8 eV are calculated by GGA+U. The MBJGGA+U calculations are performed with U=1 for $LiFePO_4$ and U=3 for $FePO_4$. Experimental data are plotted on the bottom of (c) and (d) for comparison purpose.

Physical Chemistry Chemical Physics Accepted Manuscript

Please do not adjust margins

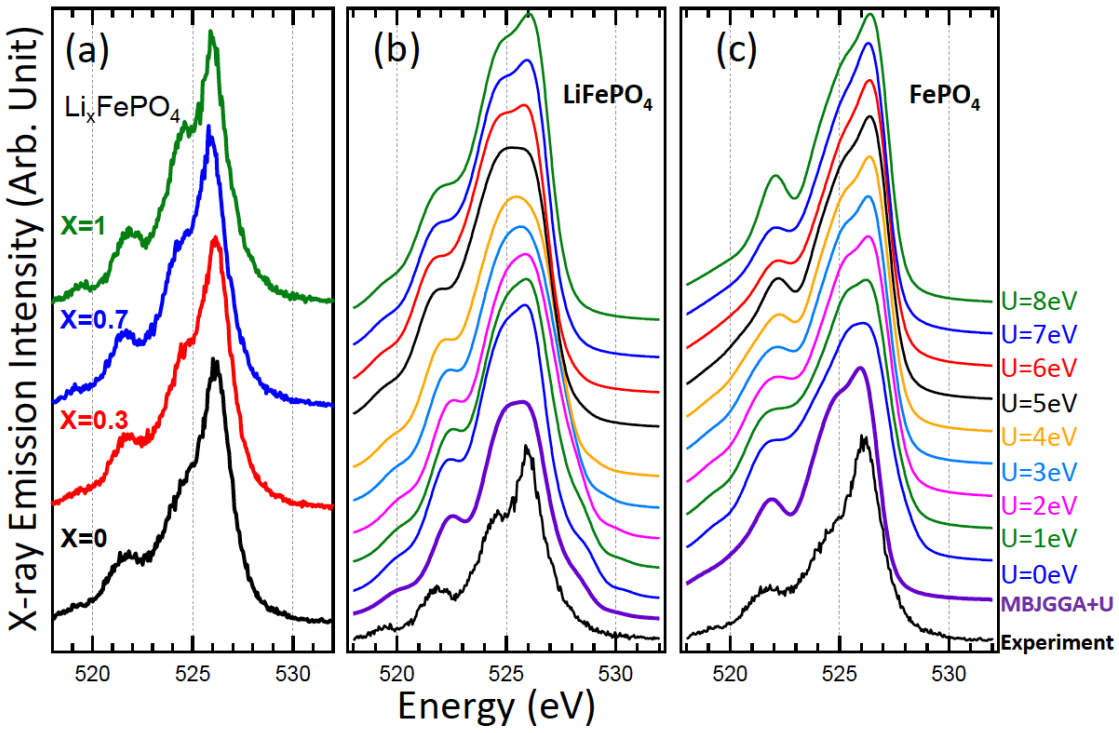

Fig.3 (a) Soft X-ray emission spectroscopy of the O-*K* edges of Li_xFePO_4 (x=0, 0.3, 0.7, 1). (b) and (c) are theoretical calculations of O-K sXES of $LiFePO_4$ and $FePO_4$, respectively. GGA+U and MBJGGA+U are calculated with the same parameters as those for Fig.2.

Physical Chemistry Chemical Physics Accepted Manuscript

This journal is © The Royal Society of Chemistry 20xx

Please do not adjust margins

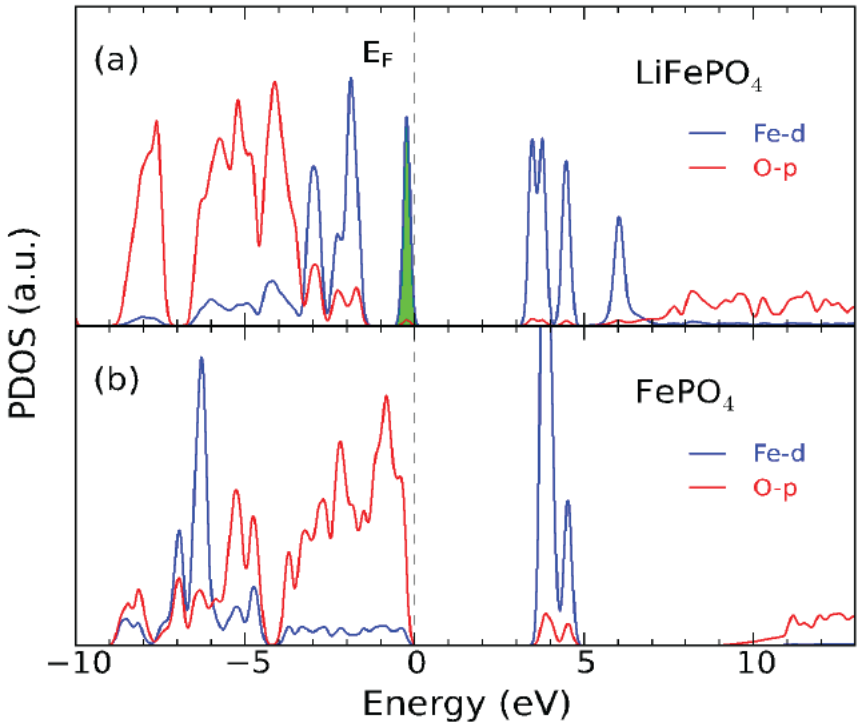

Fig.4 Spin-polarized pDOS of Fe-3*d* (4 atoms) and O-2*p* pDOS (16 atoms) of (a) $LiFePO_4$ and (b) $FePO_4$. The distinct occupied Fe-3d state close to the Fermi level (filled) is the state of electrons with the minority spin.

Physical Chemistry Chemical Physics Accepted Manuscript

Please do not adjust margins

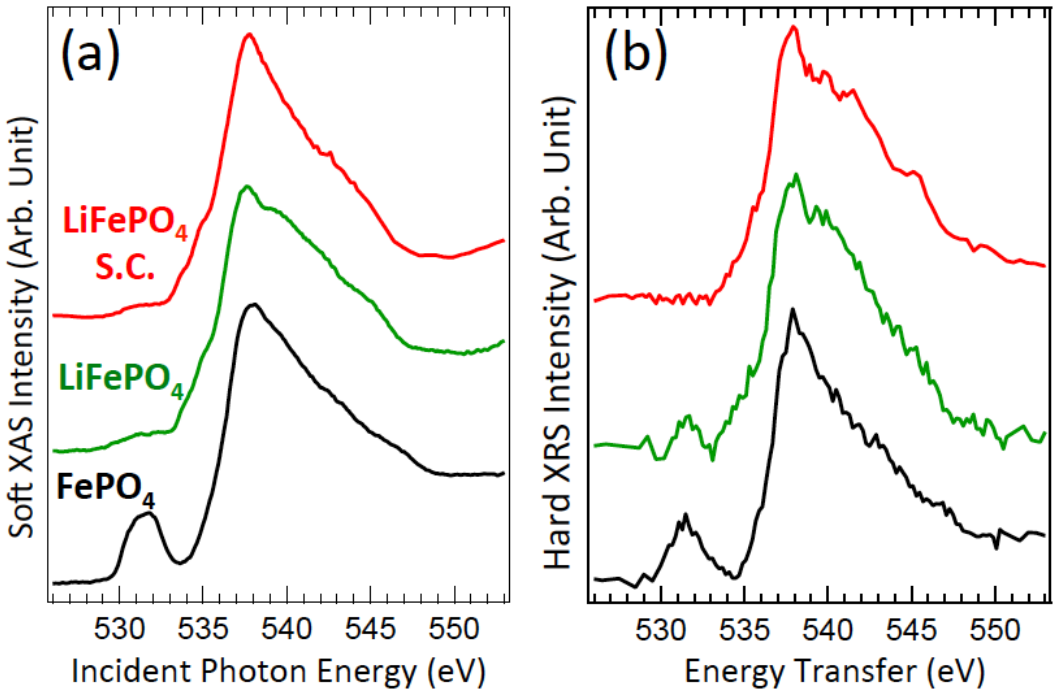

Fig.5 Soft X-ray absorption spectroscopy (a) and hard X-ray Raman spectroscopy (b) of the O-*K* edges of $FePO_4$ nanoparticles (black), $LiFePO_4$ nanoparticles (green), and $LiFePO_4$ single crystals (red). hXRS of the $LiFePO_4$ single crystal show no pre-edge feature, indicating the very weak pre-edge feature in $LiFePO_4$ is from surface effect. The strong pre-edge feature of $FePO_4$ indicates the Fe-*3d* unoccupied states below the broad O-*2p* bands.

Physical Chemistry Chemical Physics Accepted Manuscript

This journal is © The Royal Society of Chemistry 20xx

Please do not adjust margins

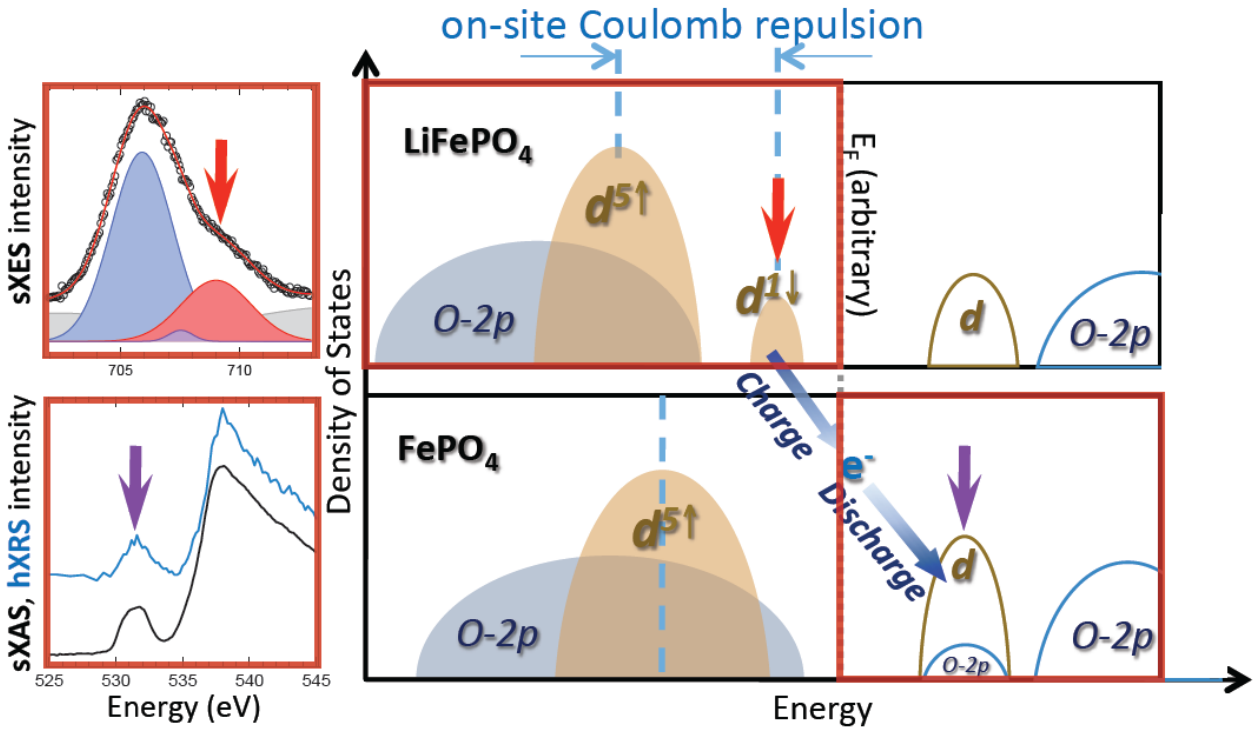

Fig. 6 Summary of the sXES, sXAS, hXRS results and schematic of the electronic state distributions in $LiFePO_4$ and $FePO_4$. The red arrows indicate the highest occupied (sXES) states of $LiFePO_4$, where electrons will be removed from during the electrochemical charge process. The purple arrows indicate the lowest unoccupied (sXAS and hXRS) states of $FePO_4$, where electrons will be filled into during the electrochemical discharge process. It is clear that both of these critical states are of Fe-*3d* character.

Physical Chemistry Chemical Physics Accepted Manuscript

Please do not adjust margins